IEEE Access
Multidisciplinary | Rapid Review | Open Access Journal

Received May 9, 2019, accepted May 23, 2019, date of publication May 27, 2019, date of current version June 17, 2019.

Digital Object Identifier 10.1109/ACCESS.2019.2919384

Fast S-Parameter TAN Model of n-Port Lumped Structures

C. CHOLACHUE[1,2], (Student Member, IEEE), B. RAVELO[2], (Member, IEEE), A. SIMOENS[1], AND A. FATHALLAH[1]

[1]Federal-Mogul Systems Protection SAS, 60800 Crépy-en-Valois, France
[2]Normandy University UNIROUEN, ESIGELEC, IRSEEM EA 4353, F-76801 Saint-Étienne-du-Rouvray, France

Corresponding author: C. Cholachue (christelngounou@yahoo.com)

ABSTRACT This paper deals with the fast S-parameter modeling of multi-port lumped structures. The developed model is based on unfamiliar formalism using the tensorial analysis of networks (TAN). The modeling methodology is described with the general abstract topology and different application cases. The methodology consists, first, in elaborating the equivalent graph topology of the considered problem. Then, it is followed by the TAN mathematical abstraction, including, successively, the branch and mesh space analyses. The problem metric can be written with the tensorial Ohm's law expressed in function of the covariant voltage, contravariant current, and the twice covariant impedance in the mesh spaces. The equivalent Z-matrix of the considered multi-port structure is established from an innovative reduction method of the mesh impedance. The S-parameter model is extracted from the Z-to-S matrix transform. The effectiveness of the established fast S-parameter TAN modeling is validated with three cases of proof of concept constituted by TT-cell, the TTT-cell two-port circuit, and four-port structure inspired from the 3D coaxial shielded cable. As expected, an excellent agreement between the S-parameters calculated from the TAN model and simulated from the commercial tools from DC to some hundred's megahertz is obtained. In the future, the developed model is outstandingly beneficial for fast and accurate applications notably for the conduced shielded cable electromagnetic compatibility analysis.

INDEX TERMS Circuit theory, cable shielding, S-parameter modeling, tensorial analysis of networks (TAN).

I. INTRODUCTION

With the increase of integration density, the interconnect connectors and cables are omnipresent and constitute a key element of electrical and electronic systems as automotive, aeronautics and spatial engineering's [1]–[7].

The undesired environmental effects as the electromagnetic compatibility (EMC) perturbations must be taken into account during the design phase [1], [5], [6]. Therefore, behind the technological design progress and the increase of the design complexity, the electrical behavior and EMC prediction become a crucial problem and have an important role for the overall system performance [1], [5]–[7]. Different measurement and simulation techniques have been deployed as standard approaches for the EMC investigation [4], [5]. Relevant analysis method [8] and optimized design [9] of shielding effectiveness are required against the undesirable EMC perturbations.

A transmission line approach basic theory was developed for the analytical investigation of the coaxial cable shields [10], [11]. The transfer impedance is among the central parameter for assessing the cable shield performance [12]. Test method international standards as IEC 62153 [13] are imposed to measure the transfer impedance. Nevertheless, similarly to most of EMC tests, the transfer impedance measurement techniques as triaxial cell-based tests [4], [5], [13], [14] are practically expensive. Therefore, with the PC revolutionary progress, popular simulation tools as HFSS® [15], CST MWS® [16] and ADS® [17] allowing to perform connector and cable virtual EMC tests have been commercialized and becoming new reference tools for the electrical, electronic and EMC engineers. But because of the misunderstanding basic mechanism, pre-processing and computation time costs, the full wave 3D simulations

The associate editor coordinating the review of this manuscript and approving it for publication was Huapeng Zhao.

as the finite element method approach [18] are not enough in electrical engineering. Furthermore, the prediction of the EMC parameters as the transfer impedance and the shielding effectiveness remain an open challenge when dealing with a particularly wide frequency band. Further research work is also needed for physical mechanism understanding about the EMC effects appearing around the tubular structures as connectors and cables [6].

For this reason, the S-parameter approach [19]–[25] constitutes an open gateway for the RF and microwave frequency range analyses. The S-matrix approach is assumed by the microwave engineers as a key parameter for the equivalent lumped circuit modeling of discontinuities [20], [21] and various microwave devices [22], [23]. However, the analytical calculation and elaboration of the S-parameters remain a fastidious task for the electrical, electronic and EMC engineers. Generally, the classical analytical processes may require series of impedance, admittance and transfer matrices.

Dealing with this analytical bottleneck, a fast and efficient S-parameter model based on the tensorial analysis of networks (TAN) formalism is developed in this paper. In state of the art, the TAN was initiated by Kron in 1930s for the electrical machine modeling. Then, the TAN was extended by Maurice and his team for analyzing and treating the problem of EMC electronic complex system analysis [27]–[30]. Then, based on the TAN formalism, calculation method of the S-parameters of printed circuit board (PCB) electrical interconnect was also proposed [31], [32]. By proceeding with the Kron's method, the S-parameter problem was transposed as the mesh current determinations. But the S-parameter analytical formulations introduced in [31], [32] are limited to calculate only one reflection and one transmission coefficients whatever the system. It means that several repetitions of analytical calculations are necessary when the number of ports is increasing.

To overcome this lack of methodologic success, a fast calculation method enabling to determine directly all the S-parameters of multiport lumped circuit is developed in the next three sections of the present paper. Section II describes the general methodology of the proposed fast and direct calculation of the S-parameter modeling. It acts as a modeling of multiport lumped circuits with the unfamiliar TAN formalism. Section III develops application cases of proof-of-concept two-port "TT" and "TTT" circuit topologies. Section IV presents another illustrative application by dealing with four-port circuit equivalent to a coaxial cable inspired from triaxial configuration. The proposed model integrates the coaxial cable transfer impedance Z_t. For a structure presenting physical length d, the developed method is dedicated to the transfer impedance corresponding to the frequency bandwidth from 0 to the maximal frequency:

$$f_{max} = c/\lambda = 10c/d, \tag{1}$$

by denoting c, the wave speed and λ, the associated wavelength. Lastly, Section V is the conclusion of the paper.

II. METHODOLOGY OF THE N-PORT LUMPED STRUCTURE S-PARAMETER MODEL

The present section introduces the methodology of the developed TAN model. After the TAN description of the problem, the S-parameter model is formulated from the impedance matrix.

A. n-PORT STRUCTURE PROBLEM FORMULATION

Fig. 1 presents a general topology of abstract multiport system with P is a strictly positive integer. This system consists of passive network constituted by R, L and C lumped elements. Under the feeding with access voltage source vector $V_{a=\{1,2,\ldots,P\}}$, the system must present access current vector $I^{a=\{1,2,\ldots,P\}}$. The determination of these two electrical parameters constitutes the key unknowns of our problem which will be going to be solved with the TAN method in the next section. They enable to determine the S-matrix model equivalent to the multiport system. It can be recalled that according to the circuit theory, the equivalent matrix impedance Z_{matrix} defined by the matrix relation:

$$[V_a] = [Z_{matrix}] \times \left[I^b\right], \tag{2}$$

or via the admittance matrix Y_{matrix} with the relation:

$$\left[I^b\right] = [Y_{matrix}] \times [V_a]. \tag{3}$$

The associated S-parameter is given by:

$$[S_{matrix}] = ([Z_{matrix}] - Z_0\,[1_P]) \times ([Z_{matrix}] + Z_0\,[1_P])^{-1}, \tag{4}$$

where Z_0 is assumed equal to 50 Ω in the present study. It represents the common reference impedance of all access port and 1_P is the P size identity matrix:

$$[1_P] = \begin{bmatrix} 1 & 0 & \cdots & 0 \\ 0 & 1 & \ddots & \vdots \\ \vdots & \ddots & \ddots & 0 \\ 0 & \cdots & 0 & 1 \end{bmatrix}. \tag{5}$$

This last relation will serve to calculate the S-parameter.

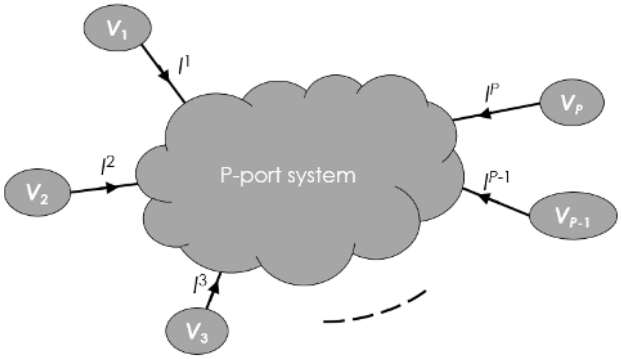

FIGURE 1. General topology of *P*-port system.

B. MODELLING METHODOLOGY OF THE PROPOSED FAST S-PARAMETER TAN

As reported in [26]–[32], the TAN formalism is implemented based on the graph topology followed by the problem metric elaboration with tensorial approach. Fig. 2 indicates the fundamental phases of the TAN approach for solving electrical problems.

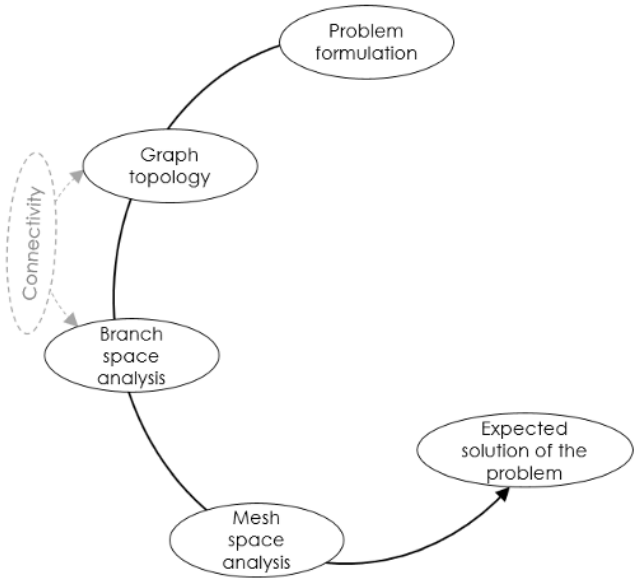

FIGURE 2. Main phases of the TAN method.

This analytical process must start with the topological analysis by identifying the quintuplet integers:

- The network number, Nw,
- The branch number, B,
- The node number, N,
- The mesh number, $M < B$,
- And the port number, $P < M$.

It is worth to recall that in the following section, the Ohm's law $V = ZI$ rewritten and implemented in tensorial notation, must respect the tensor algebra rule:

- the voltage V (noticed with a subscript as V_a) is a covariant parameter which is represented as a row vector,
- the current I (noticed with a superscript as I^b) is a contravariant parameter which is represented as a column vector,
- and the associated impedance Z must be a twice covariant parameter which is denoted with two subscripts Z_{ab} and represented as a square matrix.

1) BRANCH SPACE VARIABLES

The branch space analysis consists in expressing:

- The covariant parameter V_b represented by the branch source voltage vector:

$$[V_b] = \begin{bmatrix} V_1 & V_2 & \cdots & V_B \end{bmatrix}, \tag{6}$$

- The contravariant parameter I^b represented by the branch current vector:

$$\left[I^b\right] = \begin{bmatrix} I^1 \\ I^2 \\ \vdots \\ I^B \end{bmatrix}, \tag{7}$$

- And the twice covariant metric represented by the branch impedance matrix which is systematically a diagonal matrix for the lumped circuit with inter-branch coupling:

$$[Z_{bb}] = \begin{bmatrix} Z_{11} & 0 & \cdots & 0 \\ 0 & Z_{22} & \ddots & \vdots \\ \vdots & \ddots & \ddots & 0 \\ 0 & \cdots & 0 & Z_{BB} \end{bmatrix}. \tag{8}$$

The mesh space analysis is derived from these branch space variables via the connectivity matrix $\left[C_b^m\right]$ which will be described in the next paragraph.

2) MESH SPACE VARIABLES

The mesh space analysis consists in expressing:

- The mesh voltage is the covariant parameter U_m represented by the vector:

$$\begin{cases} [U_m] = \begin{bmatrix} U_1 & U_2 & \cdots & U_M \end{bmatrix} \\ [U_m] = \left[C_m^b\right] \times [V_b] \Rightarrow U_m = C_m^b V_b, \end{cases} \tag{9}$$

  It is worth to emphasize that the voltage vector component $U_m = 0$ in all meshes without external sources.
- Knowing that $\left[C_b^m\right] = \left[C_m^b\right]^t$, the mesh current is the contravariant parameter J^n represented by the vector:

$$\begin{cases} [J^n] = \begin{bmatrix} J^1 \\ J^2 \\ \vdots \\ J^M \end{bmatrix} \\ [J^n] = \left[C_b^n\right] \times \left[I^b\right] \Rightarrow J^n = C_b^n I^b, \end{cases} \tag{10}$$

- And the twice covariant metric represented by the mesh impedance matrix:

$$\begin{cases} [Z_{mn}] = \begin{bmatrix} Z_{11} & Z_{12} & \cdots & Z_{1M} \\ Z_{21} & Z_{22} & \cdots & Z_{2M} \\ \vdots & \vdots & \ddots & \vdots \\ Z_{M1} & Z_{M2} & \cdots & Z_{MM} \end{bmatrix} \\ [Z_{mn}] = \left[C_m^b\right] \times [Z_{bb}] \times \left[C_n^b\right] \Rightarrow Z_{mn} = C_m^b Z_{bb} C_n^b. \end{cases} \tag{11}$$

The fundamental metric of the problem can be formulated by the tensorial compact Einstein relation:

$$\left[J^n\right] = \left[Y^{nm}\right] \times [U_m] \Rightarrow J^n = Y^{nm} U_m, \tag{12}$$

where:

$$\left[Y^{nm}\right] = [Z_{mn}]^{-1}. \tag{13}$$

3) METHODOLOGY

Fig. 3 describes the successive steps of the analytical processes constituting the proposed fast S-parameter TAN model. This workflow indicates the overview of the overall routine algorithm to be applied to the proof-of-concept circuits in the next two sections.

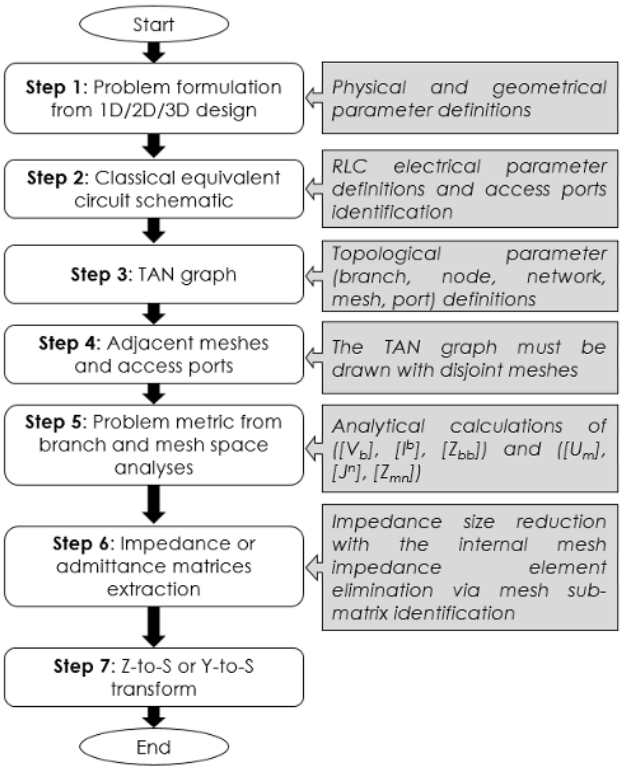

FIGURE 3. Workflow illustrating the proposed fast S-parameter TAN modeling methodology.

The starting point of the fast S-parameter modeling method consists in formulating the problem by defining the initial parameters which can be the physical, geometrical or/and electrical variables. The next steps are the classical electrical circuit representation. The medium steps are the branch and mesh space analyses elaborated in the previous paragraphs. It is noteworthy that the validity condition depend on the disjoint access meshes formulated by:

$$\begin{bmatrix} J^1 \\ J^2 \\ \vdots \\ J^P \end{bmatrix} = \begin{bmatrix} I^1 \\ I^2 \\ \vdots \\ I^P \end{bmatrix} \Leftrightarrow \left[C_b^m(1\ldots P, 1\ldots P)\right] = [1_P]\,. \quad (14)$$

The detailed description of the Step 6 analytical calculation will be explained in the next subsection.

C. Z-MATRIX AND S-PARAMETER EXTRACTIONS

The main original aspect of the developed fast S-parameter TAN model lies on the extraction of the impedance matrix from the mesh impedance $[Z_{mn}]$ expressed in equation (11). According to the circuit and system theory, the structure under study can be assumed as a P-port diagram. This type of system is usually represented by the impedance $[Z_{matrix}]$ or admittance:

$$[Y_{matrix}] = [Z_{matrix}]^{-1}\,, \quad (15)$$

which are assumed as p-size square matrices, linked by the classical definition:

$$\begin{aligned} {}^t\begin{bmatrix} V_1 \\ \vdots \\ V_p \end{bmatrix} = [Z_{matrix}] \times \begin{bmatrix} I^1 \\ \vdots \\ I^p \end{bmatrix} = [Z_{matrix}] \\ \times \begin{bmatrix} C_1^1 & \cdots & C_p^1 \\ \vdots & \ddots & \vdots \\ C_1^p & \cdots & C_p^p \end{bmatrix} \times \begin{bmatrix} J^1 \\ \vdots \\ J^p \end{bmatrix}. \end{aligned} \quad (16)$$

The equivalent impedance matrix relation is given by:

$$\begin{bmatrix} J^1 \\ \vdots \\ J^p \end{bmatrix} = \left([Z_{matrix}] \times \left[C_m^a(1\ldots p, 1\ldots p)\right]\right)^{-1} \times {}^t\begin{bmatrix} V_1 \\ \vdots \\ V_p \end{bmatrix} \quad (17)$$

The key originality of the TAN model concerns the impedance matrix from the mesh impedance defined in equation (11). For the better understanding about this impedance matrix extraction, it is worth to recall the following linear expanded expression of the mesh voltage depicted in equation (18), as shown at the bottom of the next page, which yields from (12). It means that the mesh impedance can be expanded in equation (19), as shown at the bottom of the next page.

Emphatically, the impedance matrix defined in equation (16) can be derived by expressing the mesh currents $J^{(p+1)\ldots M}$ in function of $J^{1\ldots p}$ from equations $(\Gamma_{(p+1)\ldots M})$ of linear system (18). The impedance matrix can be algebraically derived substituting the matrix relationship written in global equation (20), as shown at the bottom of the next page, into equation (18). Emphatically, the mesh impedance must be subdivided, as illustrated in equation (15), into four sub-matrices denoted:

- $[Z_A]$ having size $P \times P$,
- $[Z_B]$ having size $P \times (M\text{-}P)$,
- $[Z_C]$ having size $(M\text{-}P) \times P$,
- And $[Z_D]$ having size $(M\text{-}P) \times (M\text{-}P)$.

It yields the impedance matrix expressed as:

$$[Z_{mn}] = \begin{array}{|c|c|c|} \hline 1\ldots P \leftrightarrow & P{+}1\ldots M \leftrightarrow & \\ \hline [Z_A] & [Z_B] & \updownarrow 1\ldots P \\ \hline [Z_C] & [Z_D] & \updownarrow P{+}1\ldots M \\ \hline \end{array} \quad (22)$$

Then, the associated S-parameter determined from the Z-to-S transform is introduced in equation (4).

For the further illustration about the feasibility of the proposed S-parameter TAN model, application cases of two-port circuit will be discussed in the next section.

III. S-PARAMETER TAN INVESTIGATION OF 2-PORT LUMPED CIRCUITS

To highlight the feasibility of the developed unfamiliar model, an application case of two-port circuit based on the TTT-topology will be explored in the present section.

A. ANALYTICAL THEORY OF TTT-TOPOLOGY OF LUMPED CIRCUIT

Following the methodology described earlier in Fig. 3, the next paragraphs will focus on the graph topology, branch and mesh space TAN.

1) GRAPH DESCRIPTION

Fig. 4(a) presents the TTT-topology of the two-port circuit under study.

The excitation voltage sources V_1 and V_2 are inserted in the access branches referred by Port P_1 and Port P_2 with internal impedances Z_{01} and Z_{02}. The internal branches $I^{3\ldots9}$ are supposed presenting impedances $Z_{3\ldots9}$.

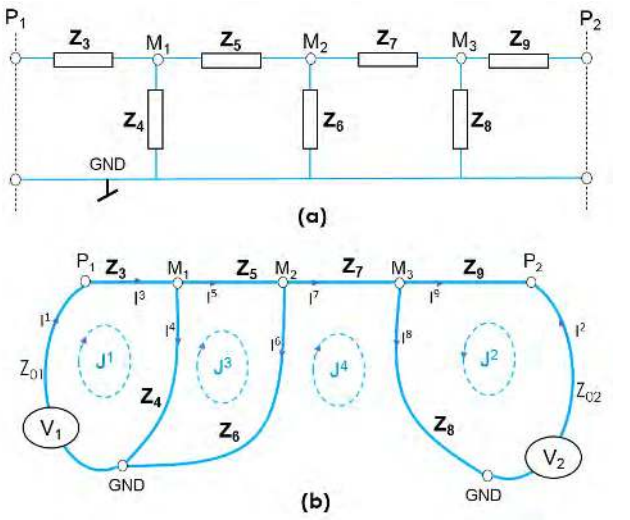

FIGURE 4. Two-port (a) classical circuit and (b) equivalent graph topology.

The TAN equivalent graph of the circuit shown in Fig. 4(a) is drawn in Fig. 4(b). It can be understood from the topological analysis that this circuit is defined with the following parameters: $Nw = 1$, $B = 9$, $N = 5$, $P = 2$ and $M = 4$.

$$\begin{cases} (\Gamma_1) \ : U_1 = Z_{11}J^1 + Z_{12}J^2 + \cdots + Z_{1p}J^p + Z_{1(p+1)}J^{p+1} + \cdots + Z_{1M}J^M \\ (\Gamma_2) \ : U_2 = Z_{21}J^1 + Z_{22}J^2 + \cdots + Z_{2p}J^p + Z_{2(p+1)}J^{p+1} + \cdots + Z_{2M}J^M \\ \vdots \\ (\Gamma_p) \ : U_p = Z_{p1}J^1 + Z_{p2}J^2 + \cdots + Z_{pp}J^p + Z_{p(p+1)}J^{p+1} + \cdots + Z_{pM}J^M \\ \hline (\Gamma_{p+1}) \ : 0 = Z_{(p+1)1}J^1 + Z_{(p+1)2}J^2 + \cdots + Z_{(p+1)p}J^p + Z_{(p+1)(p+1)}J^{p+1} + \cdots + Z_{(p+1)M}J^M \\ \vdots \\ (\Gamma_M) \ : 0 = Z_{M1}J^1 + Z_{M2}J^2 + \cdots + Z_{Mp}J^p + Z_{M(p+1)}J^{p+1} + \cdots + Z_{MM}J^M. \end{cases} \tag{18}$$

$$[Z_{mn}] = \left[\begin{array}{ccc|ccc} Z_{11} & Z_{12} & \cdots & Z_{1p} & Z_{1(p+1)} & \cdots & Z_{1M} \\ Z_{21} & Z_{22} & \cdots & Z_{2p} & Z_{2(p+1)} & \cdots & Z_{2M} \\ \vdots & \vdots & \ddots & \vdots & \vdots & \ddots & \vdots \\ Z_{p1} & Z_{p2} & \cdots & Z_{pp} & Z_{p(p+1)} & \cdots & Z_{pM} \\ \hline Z_{(p+1)1} & Z_{(p+1)2} & \cdots & Z_{(p+1)p} & Z_{(p+1)(p+1)} & \cdots & Z_{(p+1)M} \\ \vdots & \vdots & \ddots & \vdots & \vdots & \ddots & \vdots \\ Z_{M1} & Z_{M2} & \cdots & Z_{Mp} & Z_{M(p+1)} & \cdots & Z_{MM} \end{array}\right]. \tag{19}$$

$$\left.\begin{matrix} (\Gamma_{(p+1)}) \\ \vdots \\ (\Gamma_M) \end{matrix}\right\} \Rightarrow -\begin{bmatrix} Z_{(p+1)1} & \cdots & Z_{(p+1)p} \\ \vdots & \ddots & \vdots \\ Z_{M1} & \cdots & Z_{Mp} \end{bmatrix} \times \begin{bmatrix} J^1 \\ \vdots \\ J^p \end{bmatrix} = \begin{bmatrix} Z_{(p+1)(p+1)} & \cdots & Z_{(p+1)M} \\ \vdots & \ddots & \vdots \\ Z_{M(p+1)} & \cdots & Z_{MM} \end{bmatrix} \times \begin{bmatrix} J^{p+1} \\ \vdots \\ J^M \end{bmatrix}$$
$$\Leftrightarrow \begin{bmatrix} J^{p+1} \\ \vdots \\ J^M \end{bmatrix} = -\begin{bmatrix} Z_{(p+1)(p+1)} & \cdots & Z_{(p+1)M} \\ \vdots & \ddots & \vdots \\ Z_{M(p+1)} & \cdots & Z_{MM} \end{bmatrix}^{-1} \times \begin{bmatrix} Z_{(p+1)1} & \cdots & Z_{(p+1)p} \\ \vdots & \ddots & \vdots \\ Z_{M1} & \cdots & Z_{Mp} \end{bmatrix} \times \begin{bmatrix} J^1 \\ \vdots \\ J^p \end{bmatrix}. \tag{20}$$

$$\left.\begin{matrix} (\Gamma_1) \\ \vdots \\ (\Gamma_p) \end{matrix}\right\} \Rightarrow \begin{bmatrix} U^1 \\ \vdots \\ U^p \end{bmatrix} = \begin{bmatrix} Z_{11} & \cdots & Z_{1p} \\ \vdots & \ddots & \vdots \\ Z_{p1} & \cdots & Z_{pp} \end{bmatrix} \times \begin{bmatrix} J^1 \\ \vdots \\ J^p \end{bmatrix} + \begin{bmatrix} Z_{1(p+1)} & \cdots & Z_{1M} \\ \vdots & \ddots & \vdots \\ Z_{p(p+1)} & \cdots & Z_{pM} \end{bmatrix} \times \begin{bmatrix} J^{p+1} \\ \vdots \\ J^M \end{bmatrix}. \tag{21}$$

2) TAN MODELLING

The branch space analysis enables to write the branch source voltage vector, the branch current vector and the branch impedance matrix given by, respectively:

$$[V_b] = \begin{bmatrix} V_1 & V_2 & 0 & \cdots & 0 \end{bmatrix}, \tag{24}$$

$$\begin{bmatrix} I^b \end{bmatrix} = \begin{bmatrix} I^1 \\ I^2 \\ \vdots \\ I^9 \end{bmatrix}, \tag{25}$$

$$[Z_{bb}] = \begin{bmatrix} Z_{01} & 0 & 0 & \cdots & 0 \\ 0 & Z_{02} & 0 & \cdots & 0 \\ 0 & 0 & Z_3 & \ddots & \vdots \\ \vdots & \vdots & \ddots & \ddots & 0 \\ 0 & 0 & \cdots & 0 & Z_9 \end{bmatrix}. \tag{26}$$

The connectivity matrix is expressed as:

$$\begin{bmatrix} C_b^m \end{bmatrix} = \begin{bmatrix} 1 & 0 & 0 & 0 \\ 0 & 1 & 0 & 0 \\ 1 & 0 & 0 & 0 \\ 1 & 0 & -1 & 0 \\ 0 & 0 & 1 & 0 \\ 0 & 0 & 1 & -1 \\ 0 & 0 & 0 & 1 \\ 0 & 1 & 0 & 1 \\ 0 & -1 & 0 & 0 \end{bmatrix}. \tag{27}$$

The mesh voltage derived from equation (9) is transformed as:

$$[U_m] = \begin{bmatrix} V_1 & -V_2 & 0 & 0 \end{bmatrix}. \tag{28}$$

Following equation (10), the mesh impedance is given in equation (27).

3) S-PARAMETER RESULTS

The S-parameter model is derived from the impedance matrix which is calculated from mesh sub-matrices $[Z_A]$, $[Z_B]$, $[Z_C]$ and $[Z_D]$ as formulated in equations (19) and (21), as shown at the bottom of the pervious page. After the calculation of the impedance matrix from relation (23), as shown at the bottom of this page, the S-parameter analytical expression can be obtained from equation (4).

B. APPLICATION CASE 1: TT-CIRCUIT

A particular case of the TT-cell is treated in the present subsection. The validation is based on the comparison between the circuit simulation from the electronic and RF/microwave circuit simulator ADS®from Keysight Technologies®.

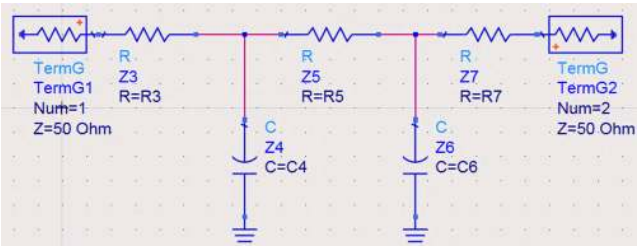

FIGURE 5. Proof-of-concept of SPICE circuit schematic.

TABLE 1. Parameters of the proof-of-concept circuit shown in Fig. 5.

Parameter	Nature	Value
Z_{01}	Resistor	R_{01}=0 Ω
Z_{02}	Resistor	R_{02}=0 Ω
Z_3	Resistor	R_3=55 Ω
Z_4	Capacitor	C_4=10 pF
Z_5	Resistor	R_5=30 Ω
Z_6	Capacitor	C_6=5 nF
Z_7	Resistor	R_7=75 Ω
Z_8	Resistor	R_8=∞
Z_9	Resistor	R_9=0

After the brief description of the proof-of-concept, the comparative results will be discussed.

1) POC DESCRIPTION

Fig. 5 depicts the proof-of-concept representing the TT-cell of the lumped two-port circuit. It is mainly constituted by resistor and capacitor components R and C. The components TermG1 and TermG2 are excitation port terminal incorporating the source reference load. They are necessary to excite the circuit. For this application case, the TAN modeling of subsection III-A was applied by defining the branch impedance parameters addressed in Table 1.

2) VALIDATION RESULTS

As numerical application, the routine algorithm of the proposed fast S-parameter TAN model inspired from the workflow of Fig. 3 was implemented in Matlab program.

The present S-parameter analyses have been performed from DC to 300 MHz. Fig. 6 plots the reflection and transmission coefficient results from the proposed TAN computations and the ADS®simulations. To highlight the comparison over the whole frequency band, linear (in top) and semi-logarithmic (in bottom) plots are presented. It can be emphasized that the TAN computation and simulation results are in excellent correlation in the whole considered

$$[Z_{mn}] = \begin{bmatrix} Z_{01}+Z_3+Z_4 & 0 & -Z_4 & 0 \\ 0 & Z_{02}+Z_8+Z_9 & 0 & -Z_8 \\ -Z_4 & 0 & Z_4+Z_5+Z_6 & -Z_6 \\ 0 & -Z_8 & -Z_6 & Z_6+Z_7+Z_8 \end{bmatrix}. \tag{23}$$

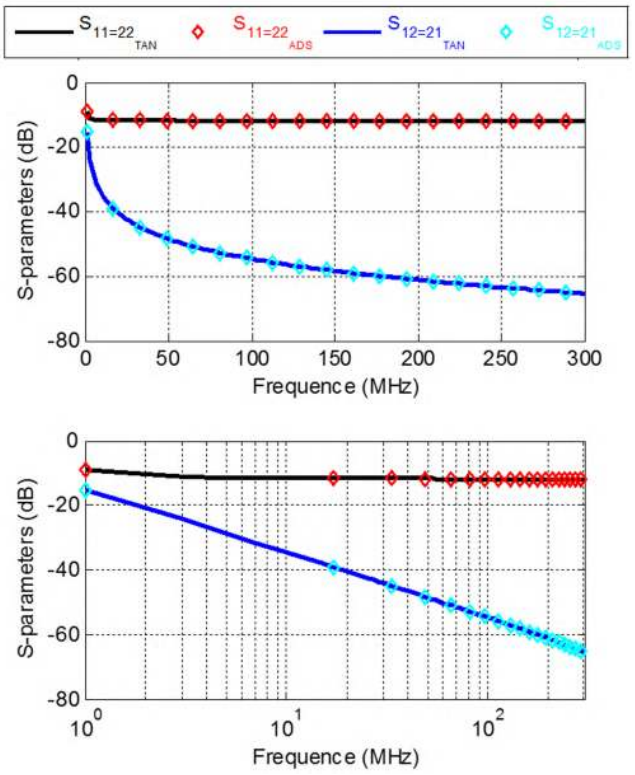

FIGURE 6. S-parameter comparative results from the circuit shown in Fig. 5.

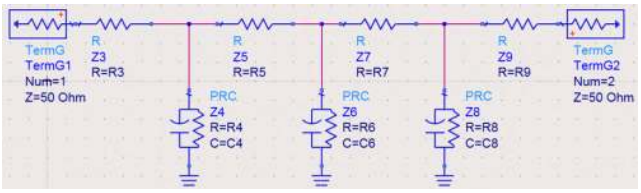

FIGURE 7. Proof-of-concept of SPICE circuit schematic with parasitic effects.

frequency band. In this figure, the TAN computed results are plotted dotted lines and the ADS®simulation results are plotted in solid lines. Acting as symmetrical passive circuit, the input and output reflection coefficients, $S_{11} = S_{22}$ and the forward and backward transmission coefficients $S_{12} = S_{21}$ are identical.

As expected, the TAN computations and the ADS simulations are in excellent correlation from DC to 300 MHz. It means that the proposed fast S-parameter model can be applied to predict the lumped circuit S-parameters in super wide band frequency. Therefore, the application case validates perfectly the feasibility of the developed S-parameter TAN model.

C. APPLICATION CASE 2: PARASITIC TTT-CIRCUIT WITH PARAMETRIC ANALYSES

In difference to the previous application case, the present one treats another passive circuit. The circuit is essentially constituted by typically parasitic effects represented by RC-parallel networks.

TABLE 2. Parameters of the proof-of-concept circuit shown in Fig. 7.

Parameter	Nature	Value
Z_{01}	Resistor	R_{01}=0 Ω
Z_{02}	Resistor	R_{02}=0 Ω
Z_3	Resistor	R_3=55 Ω
Z_4	RC-parallel network impedance	C_4=10 nF R_4=25 Ω
Z_5	Resistor	R_5=25 Ω
Z_6	RC-parallel network impedance	C_6=5 nF R_6=25 Ω
Z_7	Resistor	R_7=30 Ω
Z_8	RC-parallel network impedance	C_8=10 pF R_8=25 Ω
Z_9	Resistor	R_9=40 Ω

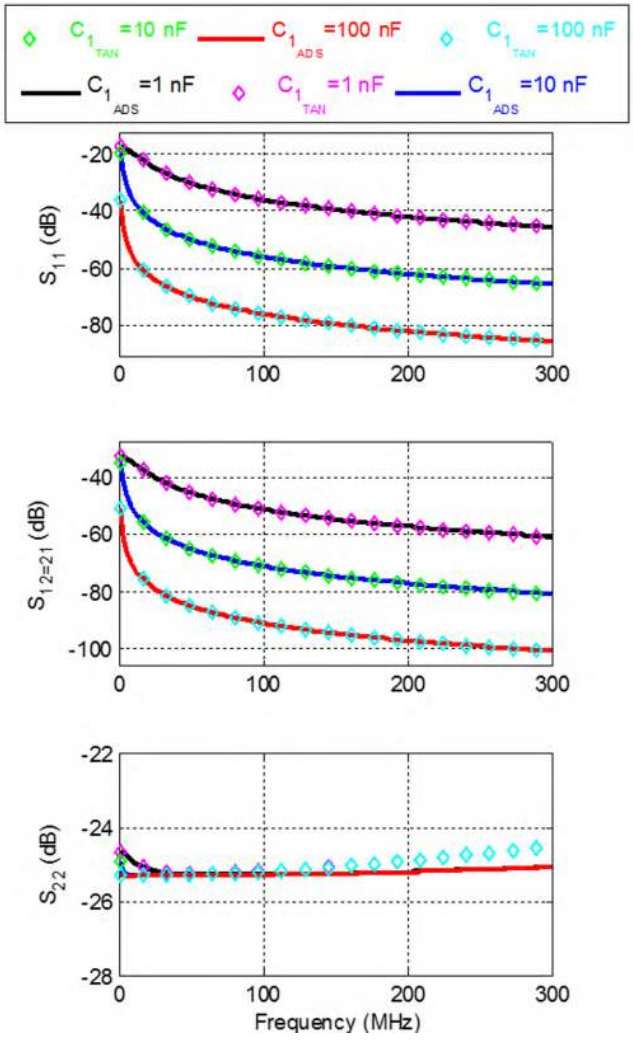

FIGURE 8. S-parameter comparison results from the circuit shown in Fig. 7.

1) POC DESCRIPTION

Fig. 7 displays the ADS schematic of the TTT-circuit proof-of-concept. It acts as a two-port circuit composed of RC-parallel network. The considered parameters of the circuit are addressed in Table 2.

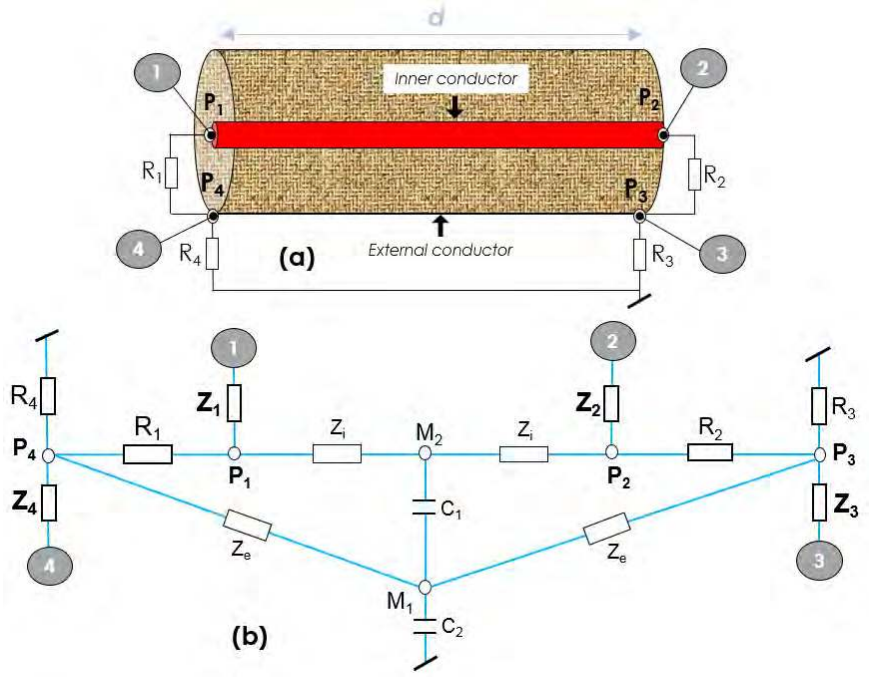

FIGURE 9. Four-port structure: (a) 3D design and (b) equivalent circuit schematic.

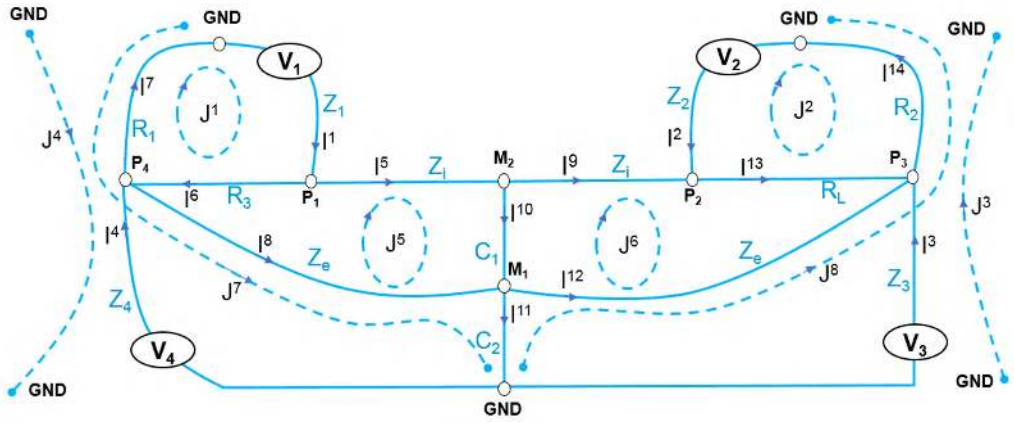

FIGURE 10. Equivalent graph of the circuit shown in Fig. 9.

2) S-PARAMETER RESULTS

Similarly, to the previous application case, the S-parameter analyses were performed from DC to 300 MHz. In addition, parametric analyses have been carried out by varying the swept values of capacitor $C_1 = \{1\text{ nF}, 10\text{ nF}, 100\text{ nF}\}$. Fig. 8 displays the obtained the comparative results from the TAN model computations (dotted lines) and ADS®simulations (solid lines). Once again, an excellent correlation between the proposed computations and commercial tool simulations have been found.

IV. S-PARAMETER TAN INVESTIGATION OF FOUR-PORT STRUCTURE

For the further understanding about the feasibility of the fast TAN S-parameter modeling more complex circuit is treated in the present section. The proof-of-concept is a four-port passive circuit inspired from the triaxial configuration of coaxial shielded cylindrical cable. Theoretical and numerical analyses will be explored based on the S-parameter comparisons.

A. THEORETICAL INVESTIGATION

After the problem description, the TAN modeling will be introduced in the next paragraphs.

1) PROBLEM FORMULATION

As explained in Fig. 9(a), in this application case, the proof-of-concept is a four-port circuit. The structure is geometrically designed as a coaxial cable. The physical parameters are defined by two cylindrical conductors having length d

TABLE 3. Parameters of the 3D structure shown in Fig. 9 and the ADS®schematic shown in Fig. 12.

Parameter	Nature	Value
Φ_i	Diameter of inner conductor	0.94 mm
Φ_d	Inner Diameter of shield	2.95 mm
Φ_e	Outer Diameter of shield	3.43 mm
t	Thickness of shield	0.24 mm
L	Cable length	10 cm
σ	Copper conductivity	17.24 nΩ/m
Z_i	RL series network impedance	R_i=1.687 Ω L_i=24.228 nH
Z_e	RL series network impedance	R_e=1.687 Ω L_e=19 nH
R_1	Resistor	50 Ω
R_2	Resistor	50 Ω
R_3	Resistor	50 Ω
R_4	Resistor	50 Ω
C_i	Capacitor	0.96 pF
C_e	Capacitor	3.81 pF

separated by an insulating dielectric structure presenting inner and external diameters Φ_i and Φ_e, respectively. The resistive loads R_1 (resp. R_2) and R_4 (resp. R_3) are connected between ports P_1-P_4 (resp. P_2-P_3) and ports P_4-GND (resp. P_3-GND). As reported in [33], [34], in low frequencies, herein, from DC up to hundred megahertz, the coaxial cable is equivalent to RLC lumped circuits. Accordingly, we considered the lumped circuit model shown in Fig. 9(b).

It is noteworthy that the source internal impedances $Z_{1...4}$ connected at port $P_{1...4}$ respectively, were considered to start the TAN modeling.

2) TAN MODELLING: BRANCH SPACE ANALYSIS

First and foremost, the graph topology of Fig. 10 has been elaborated. This topological analysis reveals that this circuit is defined with the parameters: $Nw = 1$, $B = 14$, $N = 6$, $P = 4$ and $M = 8$.

The branch space analysis enables to write the branch source voltage vector, the branch current vector and the branch impedance matrix given by, respectively:

$$[V_b] = \begin{bmatrix} V_1 & V_2 & 0 & \cdots & 0 \end{bmatrix}, \tag{29}$$

$$\begin{bmatrix} I^b \end{bmatrix} = \begin{bmatrix} I^1 \\ I^2 \\ \vdots \\ I^{14} \end{bmatrix}, \tag{30}$$

$$[Z_{bb}] = \begin{bmatrix} Z_1 & 0 & 0 & \cdots & 0 \\ 0 & Z_2 & 0 & \cdots & 0 \\ 0 & 0 & Z_3 & \ddots & \vdots \\ \vdots & \vdots & \ddots & \ddots & 0 \\ 0 & 0 & \cdots & 0 & Z_{14} \end{bmatrix}, \tag{31}$$

with $Z_5 = Z_9 = Z_i$, $Z_6 = R_3$, $Z_7 = R_1$, $Z_8 = Z_{12} = Z_e$, $Z_{10} = 1/(C_1 s)$, $Z_{11} = 1/(C_2 s)$, $Z_{13} = R_L$ and $Z_{14} = R_2$ by denoting s the Laplace variable.

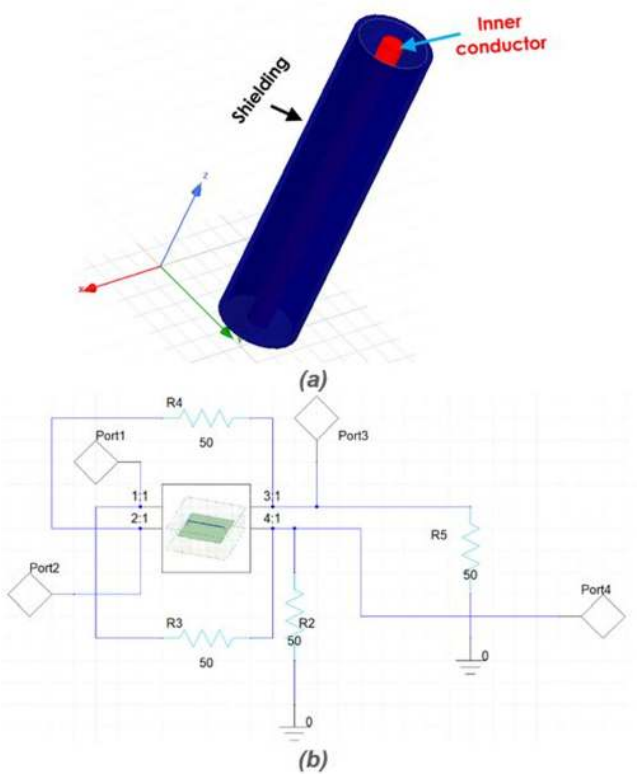

FIGURE 11. HFSS®(a) 3D and (b) hybrid structure design of the proof-of-concept structure introduced in Fig. 9.

3) TAN MODELLING: MESH SPACE ANALYSIS

The connectivity matrix related to the branch and mesh currents of the graph of Fig. 10 is expressed as:

$$\left[C_b^m\right] = \begin{bmatrix} 1 & 0 & 0 & 0 & 0 & 0 & 0 & 0 \\ 0 & -1 & 0 & 0 & 0 & 0 & 0 & 0 \\ 0 & 0 & 1 & 0 & 0 & 0 & 0 & 0 \\ 0 & 0 & 0 & -1 & 0 & 0 & 0 & 0 \\ 0 & 0 & 0 & 0 & 1 & 0 & 0 & 0 \\ 1 & 0 & 0 & 0 & -1 & 0 & 0 & 0 \\ 1 & 0 & 0 & -1 & 0 & 0 & -1 & 0 \\ 0 & 0 & 0 & 0 & -1 & 0 & 1 & 0 \\ 0 & 0 & 0 & 0 & 0 & 1 & 0 & 0 \\ 0 & 0 & 0 & 0 & 1 & -1 & 0 & 0 \\ 0 & 0 & 0 & 0 & 0 & 0 & 1 & -1 \\ 0 & 0 & 0 & 0 & 0 & -1 & 0 & -1 \\ 0 & -1 & 0 & 0 & 0 & 1 & 0 & 0 \\ 0 & -1 & 1 & 0 & 0 & 0 & 0 & -1 \end{bmatrix}. \tag{32}$$

To perform the computation, the mesh voltage associated to the graph sketched in Fig. 9 can be written as following equation (9):

$$[U_m] = \begin{bmatrix} V_1 & -V_2 & V_3 & -V_4 & 0 & 0 & 0 & 0 \end{bmatrix}, \tag{33}$$

and the mesh impedance $[Z_{mn}]$ can be calculated from equation (11). Then, the mesh sub-matrices $[Z_A]$, $[Z_B]$, $[Z_C]$ and $[Z_D]$ can be deduced as aforementioned in previous paragraph

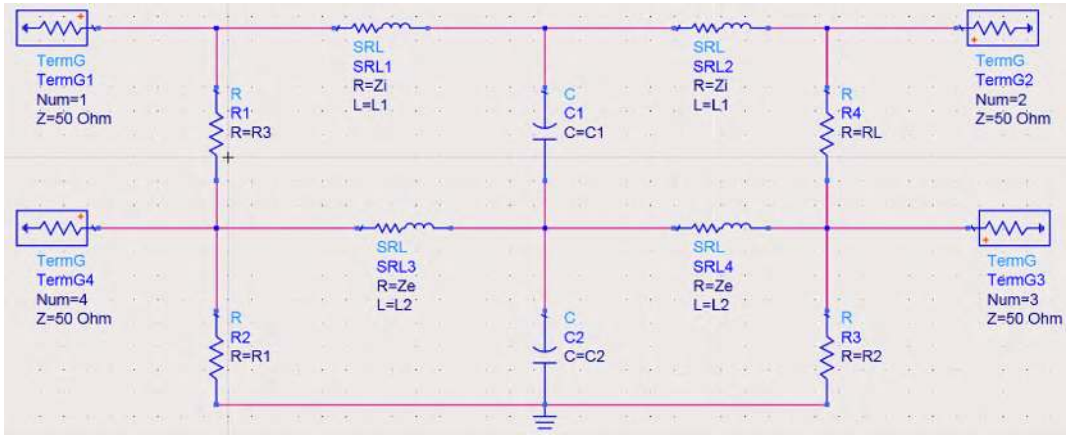

FIGURE 12. ADS®schematic of the proof-of-concept four-port circuit.

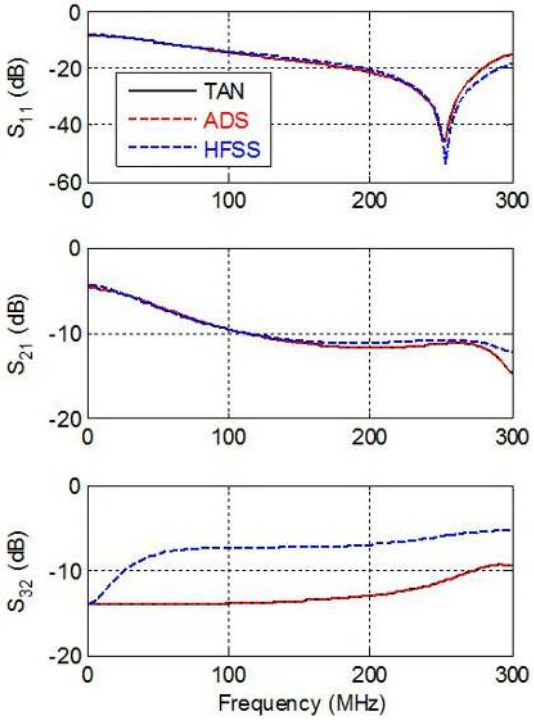

FIGURE 13. Linear plot of S-parameter comparisons from HFSS®full wave simulations, ADS®simulations and TAN computations of the proof-of-concept circuit shown in Fig. 11.

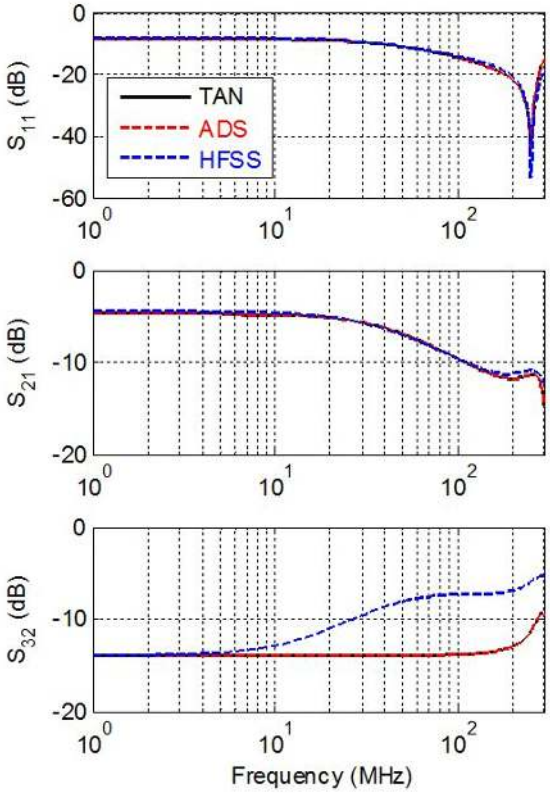

FIGURE 14. S-parameter comparisons from HFSS®full wave simulations, ADS®simulations and TAN computations of the proof-of-concept circuit shown in Fig. 11.

II-C. Afterwards, the impedance matrix can be determined from relation (23). In the final step, the targeted S-parameter model can be obtained from equation (4).

B. NUMERICAL APPLICATION WITH FULL WAVE SIMULATED VALIDATION RESULTS

The present subsection is focused on the validation of the developed fast TAN S-parameter model with circuit and full wave simulations. After description of the equivalent circuit proof-of-concept, the simulated and computed S-parameters will be compared and discussed.

1) POC DESCRIPTION

Fig. 11(a) depicts the HFSS®3D design of the coaxial cable. Fig. 11(b) shows the hybrid circuit design integrating the HFSS®full wave simulation results as a touchstone black box. Similar to the model suggested in [33-34], the lumped equivalent model of the coaxial cable constituted by the R, L and C lumped elements of the simulated ADS®circuit schematic shown in Fig. 12 was calculated. Knowing these

TABLE 4. Performances comparison.

Criterion	HFSS®	ADS®	Proposed TAN model
Design	- Possibility to design 2D and 3D configuration of coaxial cables - Do not allow to analyze large size structure	- Design environment enabling to consider lumped and distributed circuit configurations - Cannot design 2D and 3D configurations of coaxial cables	- Representation of coaxial cables with their equivalent graph as a multidimensional circuit with compact tensorial formulation of the problem metric
Pre-processing	- About 1h	- Some minutes	- Some seconds
Computation time Operation frequency	- Tens minutes - Do not allow the very low frequency analyses - Possibility to operate up to several gigahertz	- Few milliseconds - Low and high frequencies up to several GHz and even more	- Few milliseconds - Low and high frequencies up to several GHz and even more

numerical parameters, TAN Matlab computations, simulations have been run in the ADS®and HFSS®environments. The obtained results are discussed in the next paragraph.

For the present application case, the considered numerical parameters are addressed in Table 3. In the first main row, the physical and geometrical parameters of the cable based on the standard RG58 are presented. In the other main row, the electrical parameters calculated from the equivalent circuit model [33], [34] are presented.

2) VALIDATION RESULTS

Fig. 13 and Fig. 14 display the linear and semi-logarithmic plots of the reflection and transmission parameter comparisons.

Once again, even with four-port circuits, an excellent correlation is realized between TAN and ADS®. It can be found that slight discrepancies can be noticed between the TAN and HFSS®S-parameter behaviors hundred megahertz between. The present main differences are clearly due to the considered lumped circuit model, which is typically limited to tens megahertz, but not due to the TAN model itself.

3) DISCUSSION ON THE ADVANTAGES AND WEAKNESSES

The unfamiliar TAN modeling presents potential of advantages compared to many other electrical circuit analysis methods. As illustrated in Table 4, it presents considerable advantages compared to existing the commercial simulation tools ADS®and HFSS®.

V. GENERAL CONCLUSION

A computational method based on the fast TAN S-parameter modeling is developed for multi- or n-port lumped circuits. The typically electrical engineers' unfamiliar method was applied to different application cases of multi-port lumped circuits.

The analytical way illustrating the fast TAN S-parameter model is described following the Kron's formalism [26] which was suggested to the EMC modeling of complex system [27]. The originality of the performed work can be understood with the following descriptive summary:

1) The modeling was initially explained with the definition of the general configuration of the problem represented by the multi-port system. It was described the methodology of the TAN formalism from the branch, mesh, impedance matrix and S-parameter extraction.
2) The feasibility of the fast TAN S-parameter modeling was illustrated with two- and four-port proof-of-concept circuits.
3) Satisfactory validation results of reflection and transmission coefficients have been found by considering commercial simulation tools. The model is in excellent agreement with lumped circuit simulations.
4) The main advantages and drawbacks of the proposed model are discussed.

In the continuation of this study, the TAN S-parameter modeling will be applied to application cases of distributed structures. In this optic, TAN models with consideration of higher frequencies up to several gigahertz based on the Kron-Branin method [31], [32] is in progress.

ACKNOWLEDGMENT

The authors address a grateful thank to Dr. Olivier Maurice from Ariane Group for his help and fruitful discussion to develop the Kron's formalism based tensorial analysis of networks (TAN) fast S-parameter model.

REFERENCES

[1] E. P. Fowler, "Cables and connectors—Their contribution to electromagnetic cohpatibility," in *Proc. IEEE Int. Symp. Rec. Electromagn. Compat.*, Anaheim, CA, USA, Aug. 1992, pp. 329–333.
[2] C. Maul and J. W. McBride, "A model to describe intermittency phenomena in electrical connectors," in *Proc. 48th IEEE Holm Conf. Elect. Contacts*, Orlando, FL, USA, Oct. 2002, pp. 165–174.
[3] R. El Abdi, A. Beloufa, and N. Benjemaâ, "Contact resistance study of high-copper alloys used in power automotive connectors," *Proc. Inst. Mech. Eng., D, J. Automobile Eng.*, vol. 222, no. 8, pp. 1375–1383, Aug. 2008.
[4] Y.-Y. Luo, J.-Y. Yang, Y.-L. Ren, Y.-L. Zhang, and W.-J. Li, "Simulation and experimental study on plug and pull characteristic of electrical connector contact," *Chin. J. Eng. Des.*, vol. 24, no. 2, pp. 168–173, 2017.
[5] A. Morriello, T. M. Benson, A. P. Duffy, and C. F. Cheng, "Surface transfer impedance measurement: A comparison between current probe and pull-on braid methods for coaxial cables," *IEEE Trans. Electromagn. Compat.*, vol. 40, no. 1, pp. 69–76, Feb. 1998.
[6] L. K. Warne, W. L. Langston, L. I. Basilio, and W. A. Johnson, "First principles cable braid electromagnetic penetration model," *Prog. Electromagn. Res. B*, vol. 66, pp. 63–89, Jan. 2016.
[7] B. Ravelo, "Behavioral model of symmetrical multi-level T-tree interconnects," *Prog. Electromagn. Res.*, vol. 41, pp. 23–50, 2012.

[8] A. Mushtaq, S. Frei, K. Siebert, and J. Bärenfänger, "Analysis of shielding effectiveness of HV cable and connector systems used for electric vehicles," in *Proc. Int. Symp. Electromagn. Compat. (EMC EUROPE)*, Brugge, Belgium, Sep. 2013, pp. 241–246.
[9] T. Kley, "Optimized single-braided cable shields," *IEEE Trans. Electromagn. Compat.*, vol. 35, no. 1, pp. 1–9, Feb. 1993.
[10] S. A. Schelkunoff, "The electromagnetic theory of coaxial transmission lines and cylindrical shields," *Bell Syst. Tech. J.*, vol. 13, no. 4, pp. 532–579, Oct. 1934.
[11] R. B. Schulz, V. C. Plantz, and D. R. Brush, "Shielding theory and practice," *IEEE Trans. Electromagn. Compat.*, vol. EMC-30, no. 3, pp. 187–201, Aug. 1988.
[12] S. Sali, "An improved model for the transfer impedance calculations of braided coaxial cables," *IEEE Trans. Electromagn. Compat.*, vol. 33, no. 2, pp. 139–143, May 1991.
[13] *Metallic Communication Cable Test Methods—Part 4-15: Electromagnetic Compatibility (EMC)—Test Method for Measuring Transfer Impedance and Screening Attenuation–or Coupling Attenuation With Triaxial Cell*, Standard IEC 62153-4-15, Dec. 2015.
[14] B. Démoulin and L. Koné, "Shielded cable transfer impedance measurements high frequency range 100 MHz-1 GHz," in *Proc. IEEE-EMC Newslett.*, Jan. 2011, pp. 42–50.
[15] *HFSS—3D Electromagnetic Simulation Software*. Accessed: Feb. 1, 2019. [Online]. Available: https://www.ansys.com/fr-fr/products/electronics/ansys-hfss
[16] *CST—Computer Simulation Technology. 3D Electromagnetic Simulation Software*. Accessed: Feb. 1, 2019. [Online]. Available: https://www.cst.com/
[17] *ADS—RF/Microwave Electronic Circuit Simulation Software*. Accessed: Feb. 1, 2019. [Online]. Available: https://www.keysight.com/main/software.jspx?cc=FR&lc=fre&ckey=2212036&nid=-34333.804574.02&id=2212036&cmpid=zzfindeesof-ads-downloads-and-trials
[18] R. Otin, J. Verpoorte, and H. Schippers, "Finite element model for the computation of the transfer impedance of cable shields," *IEEE Trans. Electromagn. Compat.*, vol. 53, no. 4, pp. 950–958, Nov. 2011.
[19] K. Kurokawa, "Power waves and the scattering matrix," *IEEE Trans. Microw. Theory Techn.*, vol. MTT-13, no. 2, pp. 194–202, Mar. 1965.
[20] L. Zhu and K. Wu, "Unified equivalent-circuit model of planar discontinuities suitable for field theory-based CAD and optimization of M(H)MIC's," *IEEE Trans. Microw. Theory Techn.*, vol. 47, no. 9, pp. 1589–1602, Sep. 1999.
[21] R. Mittra, A. Suntives, M. S. Hossain, and J. Ma, "A systematic approach for extracting lumped circuit parameters of microstrip discontinuities from their S-parameter characteristics," *Int. J. Numer. Mod., Electron. Netw., Devices Fields*, vol. 5, no. 1, pp. 59–72, Jan./Feb. 2002.
[22] I. Timmins and K.-L. Wu, "An efficient systematic approach to model extraction for passive microwave circuits," *IEEE Trans. Microw. Theory Techn.*, vol. 48, no. 9, pp. 1565–1573, Sep. 2000.
[23] T. L. Moss and Y. Chen, "Mesh analysis for extracting the S-parameters of lumped element RF and microwave circuits," *Int. J. Elect. Eng. Educ.*, vol. 51, no. 4, pp. 330–339, Oct. 2014.
[24] J. Yan and X. Liao, "Equivalent lumped circuit model and S-parameter of indirect-heating thermoelectric power sensor," *Sens. Actuators A, Phys.*, vol. 240, pp. 110–117, Apr. 2016.
[25] F. Fesharaki, T. Djerafi, M. Chaker, and K. Wu, "S-parameter deembedding algorithm and its application to substrate integrated waveguide lumped circuit model extraction," *IEEE Trans. Microw. Theory Techn.*, vol. 65, no. 4, pp. 1179–1190, Apr. 2017.
[26] G. Kron, *Tensor Analysis of Networks*. New York, NY, USA: Wiley, 1939.
[27] O. Maurice, "Elements of theory for electromagnetic compatibility and systems," Bookelis, Aix en Provence, France, Tech. Rep., 2017.
[28] O. Maurice and A. Reineix, "Link between the free field and the elements of frontiers in a complex structure," PSA Peugeot Citroën, Vélizy Villacoublay, France, Tech. Rep. HAL hal-00265343, 2008.
[29] O. Maurice, A. Reineix, P. Durand, and F. Dubois, "Kron's method and cell complexes for magnetomotive and electromotive forces," *Int. J. Appl. Math.*, vol. 44, no. 4, pp. 183–191, 2014.
[30] O. Maurice, A. Reineix, P. Hoffmann, B. Pecqueux, and P. Pouliguen, "A formalism to compute the electromagnetic compatibility of complex networks," *Adv. Appl. Sci. Res.*, vol. 2, no. 5, pp. 439–448, 2011.
[31] B. Ravelo and O. Maurice, "Kron-branin modeling of Y-Y-tree interconnects for the pcb signal integrity analysis," *IEEE Trans. Electromagn. Compat.*, vol. 59, no. 2, pp. 411–419, Apr. 2017.
[32] Z. Xu, Y. Liu, B. Ravelo, J. Gantet, N. Marier, and O. Maurice, "Direct time-domain TAN model of 3D multilayer hybrid PCB: Experimental validation," *IEEE Access*, vol. 6, pp. 60645–60654, Oct. 2018.
[33] J. C. Rautio, "Synthesis of compact lumped models from electromagnetic analysis results," *IEEE Trans. Microw. Theory Techn.*, vol. 55, no. 12, pp. 2548–2554, Dec. 2007.
[34] P. Xiao, P.-A. Du, and B. Zhang, "An analytical method for radiated electromagnetic and shielding effectiveness of braided coaxial cable," *IEEE Trans. Electromagn. Compat.*, vol. 61, no. 1, pp. 121–127, Feb. 2019.

C. CHOLACHUE (S'19) received the master's degree in electronics and telecommunication system from University of Nice Sophia Antipolis, France, in 2017. He is currently pursuing the Ph.D. degree in EMC engineering and cable shielding modeling and characterization including the multiphysics effect with the Federal-Mogul System Protection and ESIGELEC/IRSEEM Laboratory. His research interests include the tensorial analysis of networks (TAN) based on the Kron–Branin model applied to the tubular woven, braided, and knitted shielded structures for the aeronautics, aerospace, and automobile engineering.

B. RAVELO (S'07–M'09) was born in Antananarivo, Madagascar, in 1978. He received the Dipl.Ing. degree in electronic engineering from the Graduate Polytechnic School of Engineering, Antsiranana University, Antsiranana, Madagascar, in 2000, the Professional, Research Science Master, and Ph.D. degrees from Brest University, Brest, France, in 2004, 2005, and 2008, respectively, and the Dissertation to lead research (Habilitation à Diriger des Recherches) from the University of Rouen, in 2012.

From 2001 to 2002, he was a Construction Engineer with MADIMEX Inc., Mahajanga, Madagascar. He is currently an Associate Professor with the Graduate Engineering School ESIGELEC/IRSEEM, Rouen, France. He is also a pioneer of the negative group delay (NGD) concept, theory, and their applications. He is a coauthor of more than 230 papers and regularly involved in national/international research, development, and innovation (R&D&I) projects. His current publication h-index is 18 (Reference: Google Scholar). He co-supervised and directed nine Ph.D. students whose seven Ph.D. candidates defended. He initiated, contributed actively, and invited by the committees as an Expert Reviewer of R&D&I projects funded by the national international programs, such as FUI, ANR, INTERREG VA, FP7-SME-2012, and EUREKA. His research interests include the multiphysics engineering, the tensorial analysis of networks (TAN) with the Kron's formalism, microwave engineering, electromagnetic compatibility (EMC) and interference (EMI) engineering, and signal and power integrity (SI/PI) engineering.

Dr. Ravelo is also a URSI Member. He is also a member of the Technical Committee of the Advanced Electromagnetic Symposium 2013–2019. He is regularly invited to review research papers submitted to international journals, such as the IEEE TMTT, IEEE Access, IEEE TCAS, IEEE TEMC, IEEE TIM, IEEE TIE, IEEE JMMCT, *Journal of Electromagnetic Waves and Applications*, IET CDS, IET MAP, and *International Journal of Electronics*, and international books in Wiley, Intech Science, and so on. He is also a Subject Topic Editor as a current member of the Editorial Board of *Electronics Letters* journal.

A. SIMOENS received the M.B.A. degree in executive management from Dauphine University, Paris, and the master's degree in macro-economics and international trade from UQAM, Montreal, Canada. She is currently with Federal-Mogul Systems Protection SAS.

A. FATHALLAH graduated from the École nationale supérieure des arts et industries textiles (ENSAIT), Roubaix, France. She received the master's degree in polymers chemistry from Science and Technology University (USTL), Lille, France. She is currently with Federal-Mogul Systems Protection SAS. She is also a Textile Engineer.